Electronic Supplementary Material (ESI) for RSC Advances.

Supporting Information

Insights into the competitive adsorption of pollutants on mesoporous alumina silica nano-sorbent synthesized from coal fly ash and waste aluminium foil

Aditi Chatterjee, Shahnawaz Shamim, Amiya Kumar Jana and Jayanta Kumar Basu*

*E-mail address: jkb@che.iitkgp.ernet.in (Jayanta Kumar Basu)

Department of Chemical Engineering, Indian Institute of Technology−Kharagpur, India−721302

Figs. of Contents:

Table of Contents:

Experimental

Table S1 Details of the chemicals used

Component	CAS Reg. No.	Suppliers	Purity (%)	Purification method
Sodium hydroxide	1310-73-2	Merck	97	Used as received
Sulphuric acid	7664-93-9	Merck	98	Used as received
Hydrochloric acid	7647-01-0	Merck	35	Used as received
Lead nitrate	10099-74-8	Merck	99	Used as received
Malachite green (IUPAC Name : 4-{[4-(Dimethylamino) phenyl](phenyl)methylidene}-*N*,*N*-dimethylcyclohexa-2,5-dien-1-iminium chloride)	2437-29-8	Loba Chemicals	90	Used as received

S1. Characterizing nano-sorbent

The elemental analysis of fly ash and developed adsorbent was performed by X-ray fluorescence (XRF) technique (Model: PAN analytical, Axios; The Netherlands). High

resolution X-ray diffraction (XRD) pattern, using PAN analytical diffract meter (Model: PW-3050/60; UK), at 40 kV and 30 mA with 2θ angle scanning from 10^0 to 70^0 using Cu-Kα radiation was recorded to analyze the crystallinity of raw fly ash and prepared nano-sorbent. The chemical bonds and functional groups were recognised by Fourier-Transform Infrared Spectroscopy (FTIR) (Model: Perkin Elmer spectrum 100) within the range of wavenumber from 4000 to 400 cm^{-1}, pelletizing the samples in KBr (procured from Sisco Research Laboratory Privet Limited; India). The surface area, pore diameter, pore volume and pore distribution were measured by Quantrachrome instrument (Model: AUTOSORB-1; UK) using nitrogen adsorption desorption method. The surface topology was checked by scanning electron microscopy (SEM) (Model: MERLIN ZEISS EVO 60 SEM; Germany) and high resolution electron transmission microscope image (HR-TEM) by JEM-2100 HRTEM (Model: JEOL; Japan). HR-TEM analysis was also useful to determine particle size distribution.

S1.1. XRF, XRD and FTIR analysis

The composition of coal fly ash (raw material) and SiA-2 were determined by XRF analysis. The details of XRF analysis for fly ash and SiA-2 are shown in Table S2.

Table S2 Result of XRF analysis

Components	SiO_2 (wt%)	Al_2O_3 (wt%)	Fe_2O_3 (wt%)	Na_2O (wt%)	SO_3 (wt%)	MgO (wt%)	K_2O (wt%)	CaO (wt%)
Fly ash	58.787 ± 0.01	30.422± 0.01	4.509± 0.01	0.140± 0.01	0.110± 0.01	0.707± 0.01	2.119± 0.01	0.800± 0.01
SiA-2	31.596± 0.01	59.176± 0.01	0.482± 0.01	6.754± 0.01	0.973± 0.01	0.057± 0.01	0.162± 0.01	0.141± 0.01

The XRD pattern of fly ash and SiA-2 are shown in Fig. S1a and S1b, respectively. The XRD patterns of fly ash confirm the presence of iron silicate oxide [ICDD card no. 000110262] at the peak16.906^0 corresponding to (020) facet. The peak at 21.034^0 corresponding to (211) facet represents potassium aluminium silicate [ICDD card no. 000500437].The aluminium oxide hydrate [ICDD card no. 000010259] was observed at the diffraction peak of 26.749^0 corresponding to (202) facet, 36.649^0 corresponding to (021) facet and 50.373^0 corresponding to (015) facet. The presence of silicon oxide [ICDD card no. 000110695] was proved by peak at 31.463^0 corresponding to (102) facet. Aluminium silicate (sillimanite) [ICDD card no. 000010626] was observed by diffraction peak at 33.406^0 corresponding to (220) facet, 41.180^0 corresponding to (122) facet and 60.896^0 corresponding

to (340) facet. The trace of silicon oxide (high quartz) peak at 35.891^0 corresponding to (110) plane, and silicon oxide (cristobalite) [ICDD card no. 000040379] peak at 42.58 corresponding to (211) facet, 60.239^0 corresponding to (311) facet and 68.536^0 corresponding to (214) facet are also pointed out. From the above discussion it can be concluded that sillimanite, aluminium oxide hydrate and cristobalite has predominance in the crystalline phase of fly ash.

Concurrently, the XRD pattern of SiA-2 the peak at 21.874^0 corresponding to (-201) facet depicts the presence of sodium aluminium silicate (Albite, disordered) [ICDD card no. 000100393]. The change in crystallinity was observed after the alkali treatment followed by calcination. The average crystal size analysed from Scherrer equation is 61.143 and 27.176 nm for fly ash and SiA-2, respectively.

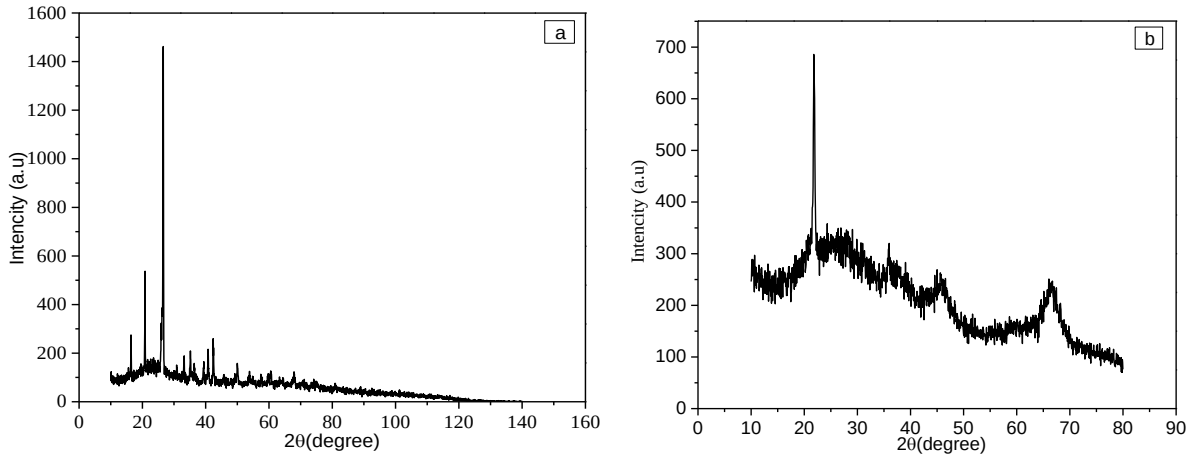

Fig. S1. XRD spectrum for (a) fly ash and (b) SiA-2

The FTIR patterns for fly ash and SiA-2 are shown in Fig. S2a and S2b, respectively. The FTIR spectrum of fly ash shown in Fig. S2a confirms the presence of T-OH (T = Si or Al) stretching at 3314.14 cm^{-1}, the existence of T-H Stretching and T-H bending at 1873.86 and 794.46 cm^{-1}, respectively. Whereas, the bands in the region of 700 – 600 cm^{-1} represents T-OH bending. At the same time T-O asymmetric stretching is confirmed by the weave number 1063.17 cm^{-1} and external tetrahedral double ring vibration was represented at 551.06 cm^{-1}.

The FTIR spectrum of SiA-2 shown in Fig. S2b, the peak at 3565.04 cm^{-1} is due to T-OH stretching, the peaks at 1634.68, 632.25, 625.24 cm^{-1} are attributed to T-OH bending. Whereas, T-O asymmetric stretching is proved by the peak at 1173.77 cm^{-1} and external tetrahedral double ring vibration is confirmed by 536.74, 580.56 cm^{-1}.[1,2] The results confirm the presence of Si-O-Al stretching in alumina silicate cluster, which resembles the powder XRD pattern of the same sample.

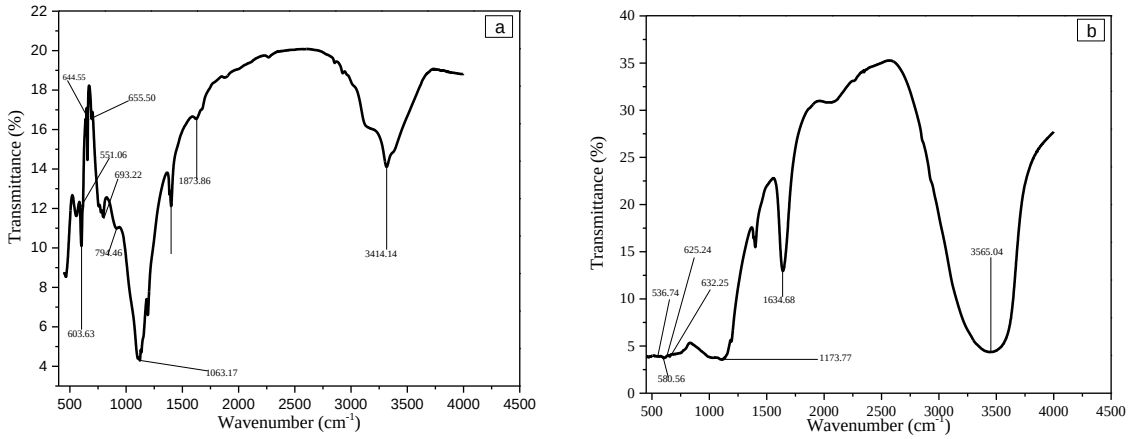

Fig. S2. FTIR spectrum of (a) fly ash and (b) SiA-2

S1.2. Morphology analysis

The surface morphology of fly ash and SiA-2 was checked by scanning electron microscopy (SEM) and the images are shown in Fig. S3 (a and b), respectively. The SEM image of fly ash shows the majority of smooth spherical particles, resemble the earlier reports,[3–6] which may be due to the presence of high silica content. Whereas, the SEM of SiA-2 depicts a flake type structure with sharp edges, which occurs due to alkaline treatment and enhancement of γ-alumina content.

The HR-TEM micrograph of SiA-2 in Fig. S4 reconfirms its flake type structure with sharp edges.

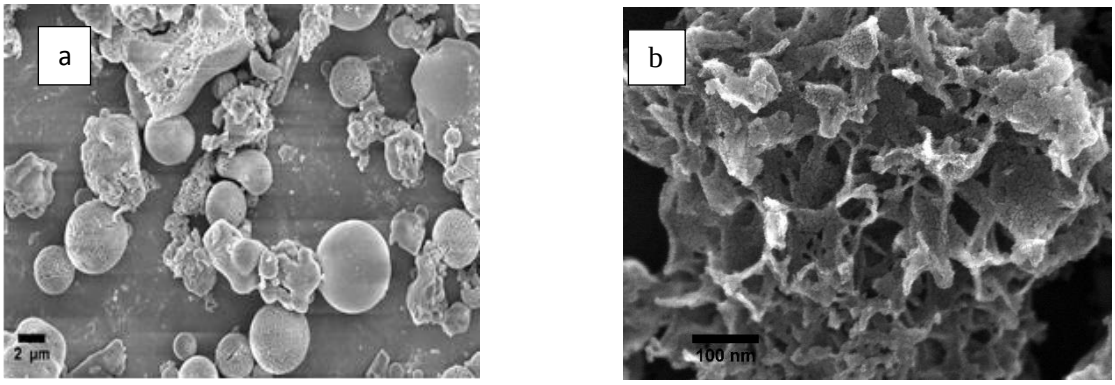

Fig. S3. SEM image of (a) fly ash and (b) SiA-2

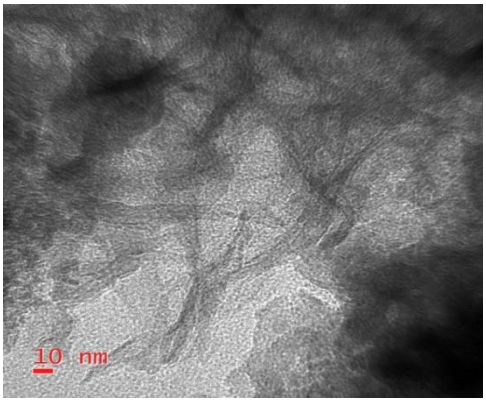

Fig. S4. HR-TEM image of SiA-2

S1.3. BET analysis of the materials

The nitrogen adsorption desorption curve of fly ash in Fig. S5a shows a type (II) hysteresis loop, that suggests disordered pore structure whereas, the narrow pore mouth offers a problem of pore blocking due to capillary condensation. On the other hand, the nitrogen adsorption desorption curve for SiA-2 in Fig. S5b gives the type (III) hysteresis loop, which ensures the slit type pore structure.[4,7] The surface area of raw fly ash was determined as 2.1 $m^2\ g^{-1}$, which drastically increased to 136.2 $m^2\ g^{-1}$ for SiA-2 due to the increase of γ-alumina content as well as porous structure. The BJH method was exploited to detect the pore diameter and pore volume. Fly ash shows a mesoporous structure with a pore diameter of 99.3 Å with a total pore volume of 0.005 cc g^{-1}. Whereas, the pore diameter and pore volume of SiA-2 was determined to be 147.1 Å and 0.50 cc g^{-1}, respectively. This phenomenon is consistent with mesoporous nature.

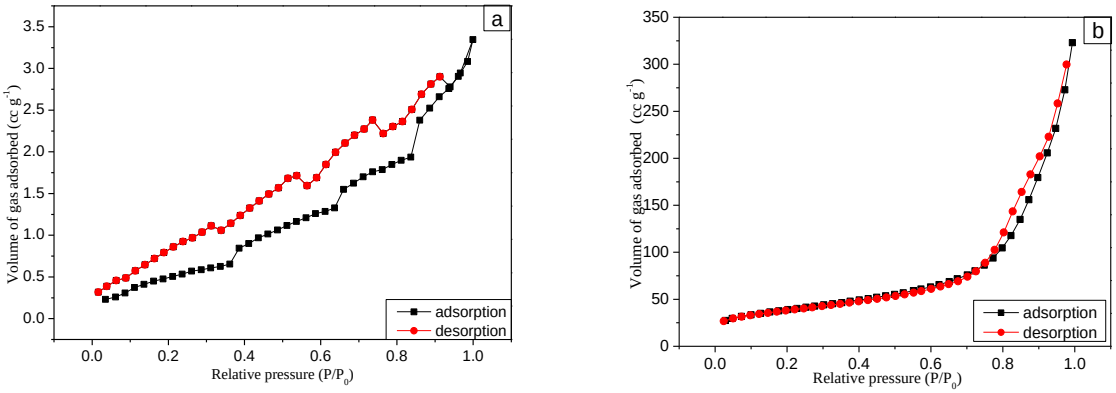

Fig. S5. The Nitrogen adsorption desorption isotherm plots of (a) fly ash and (b) SiA-2

S1.4. Point of zero charge analysis

The point of zero charge (pH_{PZC}) of SiA-2 particles was determined by measuring its Zeta potential at different pH (2-10) by using MALVERN Zetasizer instrument. The desired pH was maintained by adding dilute HCl and NaOH solution. A plot of Zeta potential versus pH is shown in Fig. S6. The result shows the pH_{PZC} of SiA-2 is at about pH 5.

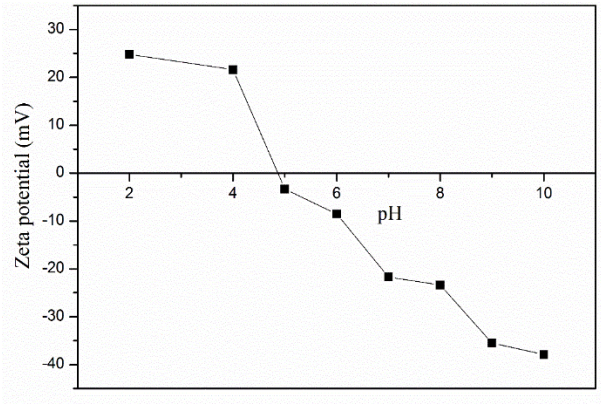

Fig. S6. Zeta potential versus pH curve of SiA-2

S2. Adsorption Experiment

The experiments were performed at 240 rpm in a mechanical shaker. The solutions were kept in conical flasks with known amount of adsorbent dosage till the equilibrium reached and the temperature was maintained in a range of 283-313K. The SiA-2 particles were separated by centrifuge at 8000 rpm for 15 min. The concentration of Pb(II) and MG were measured by Atomic Absorption Spectrophotometer (AAS) (PerkinElmer, PinAAcle 900H) and UV Visible spectrophotometer (Lambda 25, PerkinElmer, USA), respectively. The adsorption uptake at equilibrium (q_e) and instantaneous uptake (q_t) in mg g^{-1} and *%Adsorption* is calculated as described in previous literatures.[7–10]

S2.1. Effect of solution pH

In this present work, adsorption capacity of SiA-2 for Pb(II) and MG within a pH range of 2 to 8 was examined and the result is shown in Fig. S7. It is observed that the adsorption process is strongly influenced by pH of the solution. As the solution pH increases, the negative charges on the surface of the adsorbent increases and also the dissociation of the functional groups may occur on the active sites.[11] For MG the adsorption capacity remarkably increases with the increase of pH from 2 to 6, whereas the adsorption capacity becomes almost constant at above pH 6. In case of Pb(II), the adsorption capacity noticeably increases with the increase of solution pH up to 8 and precipitation occurs at above pH 8. As the MG and Pb(II) are charged species, the adsorption is strongly dependent on the point of zero

charge (pH $_{PZC}$) of the adsorbent and the molecular nature of the adsorbates. The measurement of zeta potential of SiA-2 was performed to measure the pH $_{PZC}$ and it is seen that zeta potential varies from 24.7 to -37.9, for SiA-2 in the pH range of 2 to 10. The pH $_{PZC}$ was obtained at close to pH 5 (Fig. S6). At a solution pH lower than pH $_{PZC}$ the SiA-2 surface is strongly covered with positive ions, which is not favourable for cataions. Whereas, the pH at above pH $_{PZC}$ of the adsorbent, the surface negative charges facilitates the adsorption of positive charged molecules.[11] On the other hand, the malachite green has a tendency to decolourize itself at higher pH[12], for that reason we have chosen pH 6 as working condition to ensure the reduction of malachite green through adsorption only.

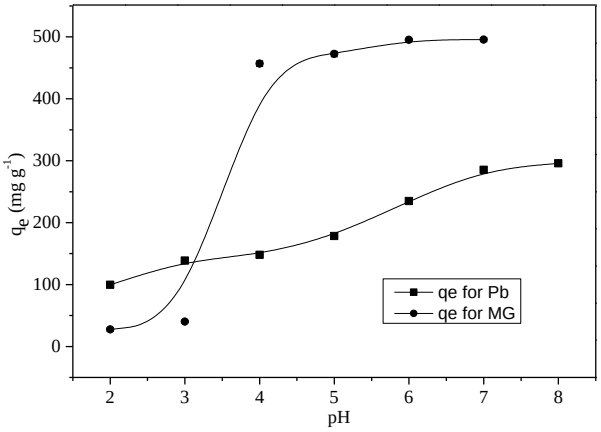

Fig. S7. Effect of pH on Pb(II) and MG adsorption (initial Pb(II) concentration: 300 mg L^{-1}; initial MG concentration: 500 mg L^{-1} ; adsorbent dosage: 1 g L^{-1}; temperature: 303 K)

S2.2. Effect of adsorption dosage

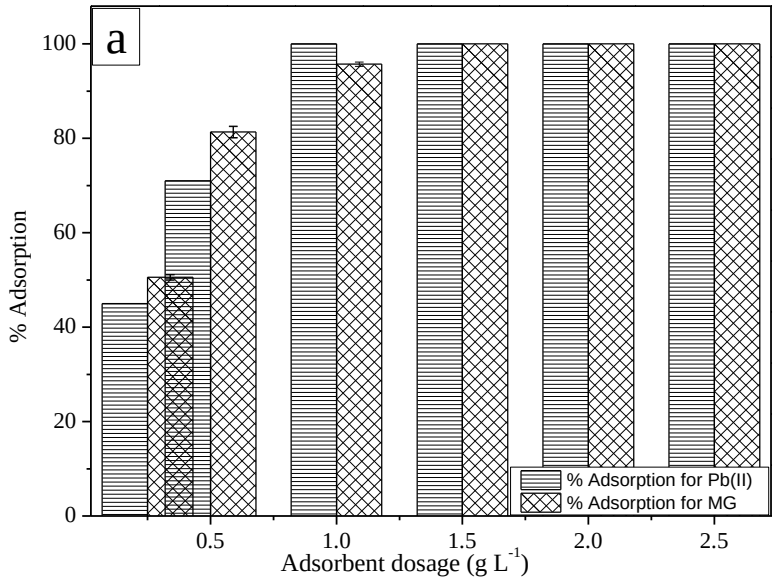

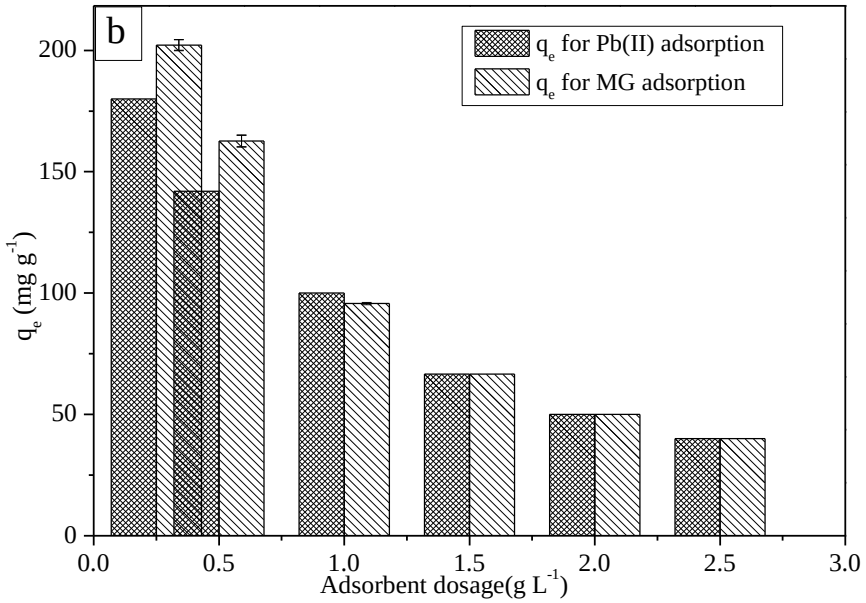

Fig. S8. Effect of adsorbent dosage on Pb(II) and MG (a) % Adsorption and (b) uptake (initial Pb(II) concentration: 100 mg L^{-1}; initial MG concentration: 100 mg L^{-1}; pH: 6; temperature: 303 K)

The effect of adsorbent dosage on adsorption uptake of Pb(II) and MG was observed by varying the adsorbent dosage from 0.25 to 2.5 g L^{-1} and at 100 mg L^{-1} initial concentration, pH 6, and 303 K temperature. It was observed form the experimental results, which are shown in Fig. S8 (a and b), the adsorption uptake decreases as adsorbent dosage increases and the *% Adsorption* increases with the increase of adsorbent dosage, up to a adsorption dosage of 1.5 g L^{-1}, after that there is no such increase of *% Adsorption*. As the adsorption dosage increases the available active sites for adsorption increases which results the increase of *% Adsorption.* On the other hand as the adsorbent dosage increases some active adsorbent site remained unoccupied, as a result the uptake by unit amount of adsorbent was less. From this experimental study it was observed that with an adsorbent dosage of 1 g L^{-1}, 100% Pb(II) adsorption was achieved and with an adsorbent dosage of 1.5 g L^{-1} 100% MG was adsorbed. This results proved that by using SiA-2 the Pb(II) and MG concentration in water can be reduced to the permissible limit.[13]

S2.3. Adorption isotherm models

The Langmuir adsorption isotherm model based on the assumption of identical and energetically equivalent active sites and monolayer adsorption, which follows the equation:

$$q_e = q_m C_e \Big/ \left(\frac{1}{b} + C_e \right) \qquad \text{(S1)}$$

Where q_e and q_m are the dye or metal equilibrium uptake (mg L^{-1}) and maximum monolayer adsorption capacity (mg L^{-1}), respectively. b (l/mg) represents Langmuir equilibrium constant. Whereas, Freundlich adsorption isotherm model describes a heterogeneous adsorption model, which is represented as:

$$q_e = K_f C_e^{1/N} \quad \text{(S2)}$$

Where K_f is the empirical constant, which is used to indicate the adsorption capacity ($mg^{1-1/N}.L^{1/N}.g^{-1}$) and N is the heterogeneity factor depending on the adsorbent and adsorbate of the system. Concurrently Temkin adsorption isotherm follows the equation:

$$q_e = (RT/b_T)\ln(AC_e) \quad \text{(S3)}$$

(RT/b_T) and A are Tempkin constants, here (RT/b_T) depends on the heat of adsorption (J mol^{-1}) and A is the equilibrium of binding constant corresponding the maximum binding energy (L g^{-1}). R and T are the universal gas constant and the absolute temperature,[14,15] respectively.

In case of binary component solution, the experimental data of equilibrium adsorption isotherm was fitted to extended Langmuir adsorption isotherm model.[16] The equation of extended Langmuir adsorption isotherm model is represented as:

$$q_{e,i} = \frac{(b_i q_{m,i} C_{e,i})}{(1 + \sum b_i C_{e,i})} \quad \text{(S4)}$$

The experimental data fitted with the adsorption isotherm models and the values of correlation coefficient and other model parameters are shown in Table S3 and S4 for single and binary component system, respectively.

Table S3 Adsorption isotherm parameters for MG and Pb(II) adsorption on SiA-2 from single component solution

Pollutants	Adsorption isotherm Model	Parameters	Values Temperature (K)		
			283	303	318
MG	Langmuir adsorption	$q_m(mg\ g^{-1})$	478.887	584.334	1655.2
	isotherm	b	0.0871	0.0350	0.008
		R^2	0.931	0.992	0.984
	Freundlich	k_f	136.955	53.996	22.809
	adsorption	n	4.358	2.721	1.302
	Isotherm	R^2	0.820	0.976	0.9751
	Tempkin adsorption	B	80.636	82.444	264.423
	isotherm	A_t	1.623	0.445	0.124

		R^2	0.903	0.942	0.922
Pb(II)	Langmuir adsorption	$q_m(mg\ g^{-1})$	193.558	291.512	326.231
	isotherm	b	0.574	0.076	0.067
		R^2	0.978	0.976	0.962
	Freundlich	k_f	159.943	110.524	112.630
	adsorption	n	30.316	5.716	5.321
	Isotherm	R^2	0.913	0.950	0.957
	Tempkin adsorption	B	6.087	4.781	5.167
	isotherm	A_t	5.9824E+10	7.5E+19	2E+20
		R^2	0.8679	0.834	0.752

Table S4 Adsorption isotherm parameters for MG and Pb(II) adsorption on SiA-2 from binary component solution

Pollutants	Adsorption isotherm Model	Parameters	Values Temperature (K)		
			283	303	318
MG	Langmuir adsorption	$q_m(mg\ g^{-1})$	103.67	391	445.03
	isotherm	b	0.085	0.016	0.038
		R^2	0.987	0.987	0.970
Pb(II)	Langmuir adsorption	$q_m(mg\ g^{-1})$	231.27	521.87	615.86
	isotherm				
		b	0.171	0.016	0.010
		R^2	0.960	0.964	0.932

S2.4. Adsorption kinetics model

The pseudo first order model[15] is established on the assumption that the rate of change of adsorption over time is directly proportional to the difference in saturation concentration and the amount of solid uptake over time. The model follows the equation:

$$\ln(q_e/(q_e - q_t)) = k_1 t \quad \text{(S5)}$$

Where, q_e (mg g^{-1}) and q_t (mg g^{-1}) are the mass of solute adsorbed on adsorbent at equilibrium and at agitation time t (min), respectively and k_1 (min^{-1}) the rate constant for pseudo-first order adsorption.

Pseudo second order equation[15] is based on the assumption that adsorption capacity is proportionate on the active sites on the adsorbent surface. The pseudo second order[15,17] model is represented by the equation:

$$\frac{1}{q_e - q_t} = \frac{1}{q_e} + k_2 t \quad \text{(S6)}$$

Here, k_2 is the adsorption rate constant. Elovich adsorption kinetics model[17] is represented by

$$q_t = \frac{1}{\beta}\ln(\beta\alpha) + \frac{1}{\beta}\ln(t) \quad \text{(S7)}$$

α and β are the initial adsorption rate (mg g^{-1} min^{-1}) and the desorption constant (mg g^{-1} min^{-1}), respectively.

Intraparticle diffusion model[17], follows the equation:

$$q_t = k_{int} t^{0.5} + C \quad \text{(S8)}$$

Where, k_{int} is the rate constant of intra-particle diffusion model and C is related to the thickness of the boundary layer. The experimental data of adsorption kinetics were fitted with the adsorption kinetic models[17], the values of correlation coefficient and other model parameters are listed in Table S5, S6 and S7 for single and binary component systems.

Table S5 Adsorption kinetics fitting parameters and correlation coefficient for MG and Pb(II) adsorption on SiA-2 from single component solution

Pollutants	Adsorption Kinetic Model	Parameters	Values	
			30 mg L^{-1}	100 mg L^{-1}
MG	Pseudo-first order model	k_1(min^{-1})	0.7690	0.8076
		q_e(mg g^{-1})	27.627	80.3815
		R^2	0.98782	0.9775
	Pseudo-second order model	k_2(g mg^{-1} min^{-1})	0.08181	0.0303
		q_e(mg g^{-1})	28.2680	81.861
		R^2	0.99702	0.98456
	Elovich kinetic model	β (mg $g^{-1}min^{-1}$)	0.93117	0.30093
		α (mg $g^{-1}min^{-1}$)	6.58877	3.33761
		R^2	0.99948	0.99143
	Intra particle diffusion model	k_{int}(mg g^{-1} $min^{-0.5}$)	0.4876	5.6758
		C	25.068	48.636
		R^2	0.9042	0.9666

Pb(II)	Pseudo-first order model	k_1(min^{-1})	0.9882	0.181
		q_e(mg g^{-1})	29.941	101.6
		R^2	0.99917	0.96543
	Pseudo-second order model	k_2(g mg^{-1} min^{-1})	0.2341	0.00228
		q_e(mg g^{-1})	30.16	114.0603
		R^2	0.99972	0.9342
	Elovich kinetic model	β (mg g^{-1}min^{-1})	1.78476	0.05547
		α (mg g^{-1}min^{-1})	368.378	157.7582
		R^2	0.99817	0.89916
	Intra particle diffusion model	k_{int}(mg g^{-1} min$^{-0.5}$)	0.0444	0.3336
		C	29.764	97.517
		R^2	0.9759	0.9954

Table S6 Adsorption kinetics fitting parameters and correlation coefficient for MG on SiA-2 from binary component solution

Pollutants	Adsorption Kinetic Model	Parameters	Values		
			30 mg L^{-1} MG with 5 mg L^{-1} Pb(II)	30 mg L^{-1} MG with 30 mg L^{-1} Pb(II)	100 mg L^{-1} Mg with 100 mg L^{-1} Pb(II)
MG	Pseudo-first order model	k_1 (min^{-1})	0.79917	0.98385	0.99893
		q_e(mg g^{-1})	27.3221	25.4750	80.1339
		R^2	0.99405	0.99395	0.35784
	Pseudo-second order model	k_2(g mg^{-1} min^{-1})	0.10232	0.15441	0.0251
		q_e(mg g^{-1})	27.8241	25.840	81.493
		R^2	0.99907	0.99807	0.99969
	Elovich kinetic model	β (mg g^{-1}min^{-1})	1.2493	1.61	0.51264
		α (mg g^{-1}min^{-1})	21.2511	1.94797	4.33299
		R^2	0.99817	0.99942	0.99991
	Intra particle diffusion model	k_{int}(mg g^{-1} min$^{-0.5}$)	0.7793	0.113	1.3973
		C	24.056	25.079	72.989
		R^2	0.9286	0.9376	0.9337

Table S7 Adsorption kinetics fitting parameters and correlation coefficient for Pb(II) adsorption on SiA-2 from binary component solution

Pollutants	Adsorption Kinetic Model	Parameters	Values		
			30 mg L^{-1} Pb(II) with 5 mg L^{-1} MG	30 mg L^{-1} Pb(II) with 30 mg L^{-1} MG	100 mg L^{-1} Pb(II) with 100 mg L^{-1} Mg
Pb(II)	Pseudo-first order model	k_1 (min^{-1})	2.3316	0.9057	0.38307
		q_e(mg g^{-1})	29.9021	26.375	99.14
		R^2	0.9995	0.99415	0.99959
	Pseudo-second order model	k_2(g mg^{-1} min^{-1})	3.48963	0.15263	0.0303
		q_e(mg g^{-1})	29.92637	26.73495	100.153
		R^2	0.99951	0.99825	0.99993
	Elovich kinetic model	β (mg $g^{-1}min^{-1}$)	3.11786	1.60016	0.68114
		α (mg $g^{-1}min^{-1}$)	6.62133	2.99596	8.68302
		R^2	0.99896	0.99502	0.99998
	Intra particle diffusion model	k_{int}(mg g^{-1} $min^{-0.5}$)	0.0401	0.0243	0.5585
		C	29.787	29.846	95.705
		R^2	0.9218	0.9081	0.9709

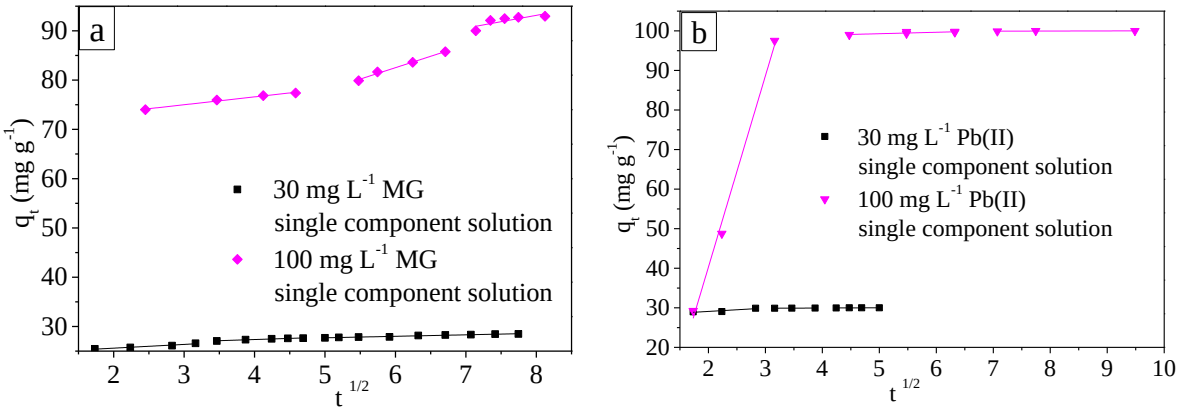

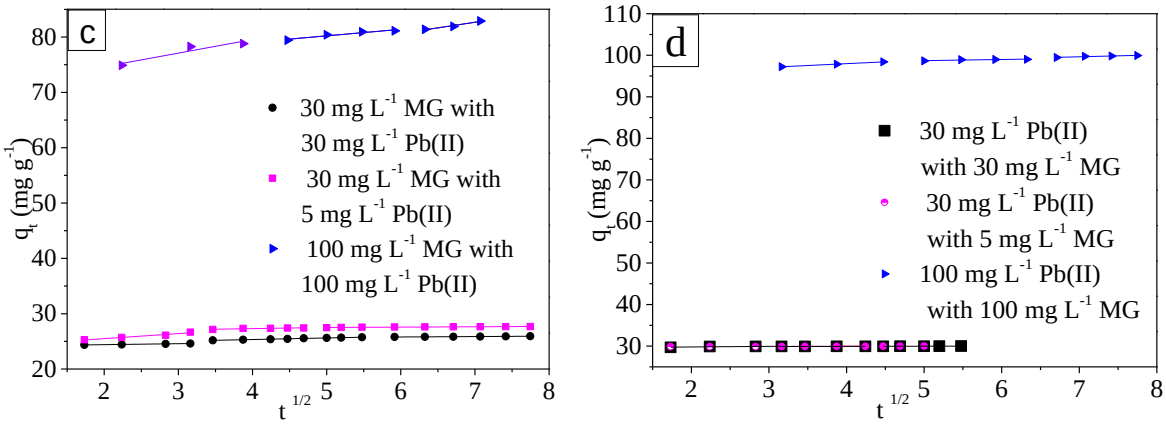

Fig. S9. Intra-particle diffusion model fit with adsorption kinetic data of (a) MG single component, (b) Pb(II) single component, (c) MG binary solution and (d) Pb(II) binary solution

S3. The mechanism of Pb(II) and MG adsorption

The mechanism of Pb(II) adsorption on alumina silica nano-sorbent can be taken into account by ion exchange process. It may be assumed that Pb(II) ions move through the pores and channels to reach the adsorption sites. The Pb(II) ions may replace the exchangeable sodium ions from sodium aluminium silicate structure[16] as shown in Equation S9 and S10. Pb(II) ions may also replace protons as shown in Equation S11 and S12. The basic dye MG will produce cationic ions (CN^+ and CNH^+) in water. The CN^+ may be adsorbed on the hydroxyl sites following Equation S13[16].

$$2\ (SiA\text{-}2)\text{-}ONa + Pb^{2+} \rightarrow ((SiA\text{-}2))\text{-}O)2Pb + 2Na^+ \quad (S9)$$

$$(SiA\text{-}2)\text{-}ONa + Pb(HCO_3)^+ \rightarrow (SiA\text{-}2)\text{-}OPb(HCO_3) + Na^{2+} \quad (S10)$$

$$2\ (SiA\text{-}2)\text{-}OH + Pb^{2+} \rightarrow ((SiA\text{-}2)\text{-}O)_2Pb + 2H^+ \quad (S11)$$

$$(SiA\text{-}2)\text{-}OH + Pb(HCO_3)^+ \rightarrow (SiA\text{-}2)\text{-}O\text{-}Pb(HCO_3) + H^+ \quad (S12)$$

$$(SiA\text{-}2)\text{-}OH + CN^+ \rightarrow (SiA\text{-}2)\text{-}O\text{-}CN + H_2O \quad (S13)$$

Table S8 Experimental range and levels of independent variables

Factor	Name	Minimum	Maximum	Coded Low	Coded High	Mean	Std. Dev.
A	Adsorbent dosage (g L^{-1})	0.25	2.50	-1 ↔ 0.90	+1 ↔ 1.85	1.37	0.44

B	initial Pb(II) concentration (mg L^{-1})	10.00	100.00	-1 ↔ 36.08	+1 ↔ 73.92	55.00	17.79
C	initial MG concentration (mg L^{-1})	10.00	100.00	-1 ↔ 36.08	+1 ↔ 73.92	55.00	17.79
D	pH	2.00	8.00	-1 ↔ 3.74	+1 ↔ 6.26	5.00	1.19
E	Temperature (K)	283.00	313.00	-1 ↔ 291.69	+1 ↔ 304.31	24.97	5.90

Table S9 Responses for different experimental runs

Run	Factor 1 A:Adsorption dosage (g L^{-1})	Factor 2 B:Initial Pb(II) concentration (mg L^{-1})	Factor 3 C:Initial MG concentration (mg L^{-1})	Factor 4 D:pH	Factor 5 E:Temperature (K)	Response 1 Pb(II) uptake (mg g^{-1})	Response 2 MG uptake (mg g^{-1})
1	1.85	73.92	73.92	6.26	304.31	39.90	39.7232
2	0.90	36.08	36.08	3.74	291.70	38.72	14.6204
3	1.37	100	55	5	298	72.67	29.0456
4	0.90	36.08	73.92	6.26	304.31	39.95	80.3821
5	1.85	73.92	36.08	3.74	291.70	8.776	14.0209
6	1.85	36.08	73.92	3.74	291.70	2.005	37.692
7	1.85	36.08	36.08	3.74	291.70	2.005	16.7207
8	0.25	55	55	5	298	161.2	53.9403
9	1.85	73.92	36.08	6.26	291.70	39.90	19.55
10	1.85	73.92	73.92	6.26	291.70	39.74	38.9345
11	1.37	55	55	2	298	0.006	35.525
12	1.85	73.92	73.92	3.74	304.31	10.86	35.8899
13	1.85	36.08	36.08	6.26	304.31	18.99	10.0865

14	0.90	36.08	73.92	3.74	304.31	38.77	76.0454
15	0.90	36.08	73.92	6.26	291.70	39.52	79.7276
16	2.5	55	55	5	298	21.96	20.789
17	1.37	55	55	5	298	39.72	36.7036
18	0.90	73.92	73.92	6.26	291.70	80.14	52.5906
19	0.90	36.08	36.08	6.26	304.31	39.84	37.4036
20	1.85	36.08	73.92	6.26	291.70	13.11	31.158
21	1.37	55	100	5	298	39.65	75.9123
22	1.37	55	55	5	298	39.72	36.7036
23	1.37	55	55	5	313	39.94	39.654
24	1.85	73.92	36.08	6.26	304.31	81.67	18.7619
25	1.85	36.08	36.08	3.74	304.31	3.010	10.8854
26	0.90	36.08	36.08	6.26	291.70	39.52	33.7113
27	1.37	55	55	5	283	31.98	30.3351
28	0.90	73.92	36.08	3.74	291.70	66.41	20.4378
29	1.85	36.08	73.92	3.74	304.31	2.009	40.97
30	0.90	73.92	73.92	3.74	291.70	71.19	22.2336
31	1.37	10	55	5	298	39.72	37.8532
32	1.37	55	55	8	298	35.78	37.3448
33	1.85	36.08	36.08	6.26	291.70	19.46	9.0183
34	0.90	36.08	73.92	3.74	291.70	38.71	68.1361

35	0.90	73.92	36.08	6.26	291.70	81.41	33.6659
36	0.90	73.92	36.08	6.26	304.31	81.16	19.2824
37	1.37	55	55	5	298	39.72	36.7036
38	1.37	55	55	5	298	39.72	36.7036
39	1.37	55	55	5	298	39.72	36.7036
40	0.90	73.92	73.92	6.26	304.31	80.83	36.2513
41	0.90	73.92	36.08	3.74	304.31	74.27	3.19625
42	1.37	55	10	5	298	39.59	6.1394
43	1.85	36.08	73.92	6.26	304.31	19.49	39.3448
44	1.37	55	55	5	298	39.72	36.7036
45	1.37	55	55	5	298	39.72	36.7036
46	1.85	73.92	36.08	3.74	304.31	34.70	19.854
47	0.905	36.08	36.08	3.74	304.31	39.87	36.13
48	1.37	55	55	5	298	39.72	36.7036
49	1.85	73.92	73.92	3.74	291.70	6.008	36.7726
50	0.90	73.92	73.92	3.74	304.31	70.85	30.3084

Table S10 ANOVA for Pb(II) uptake (Y_1)

Source	Sum of Squares	*df*	Mean Square	F-value	p-value	
Model	37691.16	20	1884.56	18.68	< 0.0001	significant
A-Adsorbent dosage	19154.29	1	19154.29	189.90	< 0.0001	
B-initial Pb(II) concentration	7021.38	1	7021.38	69.61	< 0.0001	
C-initial MG concentration	136.23	1	136.23	1.35	0.2546	
D-pH	2532.04	1	2532.04	25.10	< 0.0001	
E-Temperature	274.92	1	274.92	2.73	0.1095	
AB	379.54	1	379.54	3.76	0.0622	
AC	170.23	1	170.23	1.69	0.2041	
AD	796.42	1	796.42	7.90	0.0088	
AE	145.93	1	145.93	1.45	0.2388	
BC	117.31	1	117.31	1.16	0.2897	
BD	424.49	1	424.49	4.21	0.0494	
BE	163.39	1	163.39	1.62	0.2132	
CD	14.55	1	14.55	0.1442	0.7069	
CE	134.66	1	134.66	1.34	0.2573	

DE	1.76	1	1.76	0.0174	0.8960
A^2	3782.60	1	3782.60	37.50	< 0.0001
B^2	222.25	1	222.25	2.20	0.1485
C^2	48.00	1	48.00	0.4758	0.4958
D^2	1264.52	1	1264.52	12.54	0.0014
E^2	136.06	1	136.06	1.35	0.2549
Residual	2925.14	29	100.87		
Lack of Fit	2925.14	22	132.96		
Pure Error	0.0000	7	0.0000		
Cor Total	40616.31	49			

Table S11 ANOVA for MG uptake (Y_2)

Source	**Sum of Squares**	***df***	**Mean Square**	**F-value**	**p-value**	
Model	14682.84	15	978.86	27.20	< 0.0001	significant
A-Adsorbent dosage	2123.46	1	2123.46	59.01	< 0.0001	
B-initial Pb(II) concentration	940.04	1	940.04	26.12	< 0.0001	
C-initial MG concentration	8173.81	1	8173.81	227.15	< 0.0001	

D-pH	232.22	1	232.22	6.45	0.0158
E-Temperature	18.82	1	18.82	0.5229	0.4745
AB	1741.81	1	1741.81	48.40	< 0.0001
AC	135.82	1	135.82	3.77	0.0604
AD	367.31	1	367.31	10.21	0.0030
AE	8.69	1	8.69	0.2416	0.6262
BC	618.11	1	618.11	17.18	0.0002
BD	100.46	1	100.46	2.79	0.1039
BE	170.90	1	170.90	4.75	0.0363
CD	0.5403	1	0.5403	0.0150	0.9032
CE	8.74	1	8.74	0.2428	0.6254
DE	51.27	1	51.27	1.42	0.2409
Residual	1223.49	34	35.98		
Lack of Fit	1223.49	27	45.31		
Pure Error	0.0000	7	0.0000		
Cor Total	15906.32	49			

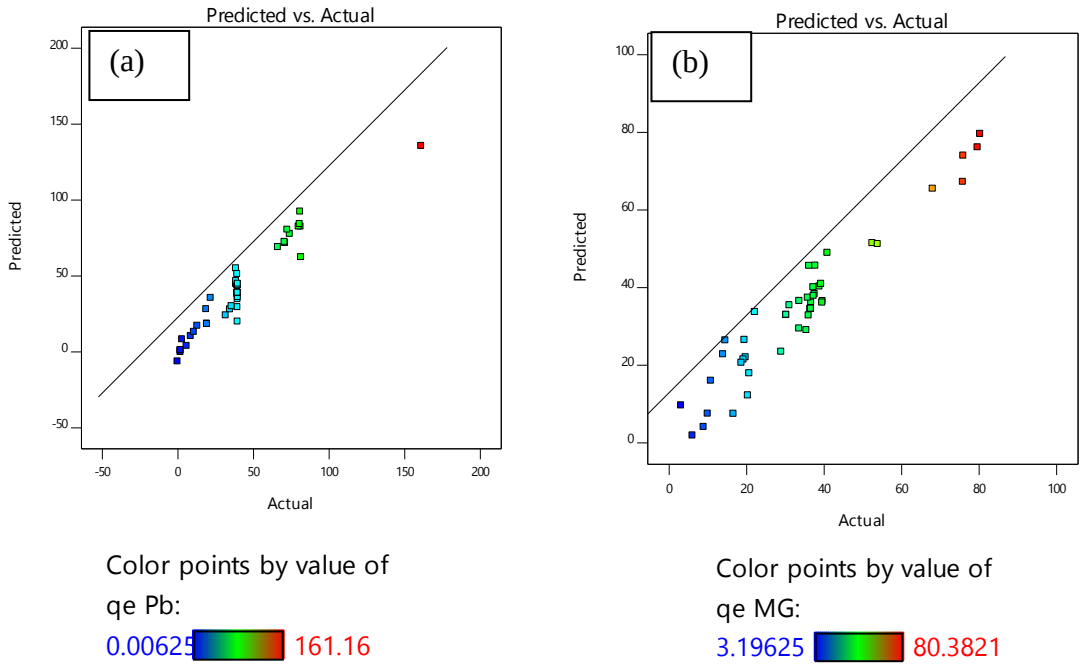

Fig. S10. Predicted vs. experimental values of adsorption uptake for (a) Pb(II) and (b) MG

S4. Thermodynamic parameters

The values of ΔH^0, ΔS^0 and ΔG^0 can be calculated from the following equations:

$$\Delta G^0 = -RT \ln K_d \quad \text{(S14)}$$

$$K_d = q_e / C_e \quad \text{(S15)}$$

$$\ln K_d = \left(-\Delta H^0 / RT\right) + \left(\Delta S^0 / R\right) \quad \text{(S16)}$$

$$\Delta S^0 = \left(\left(\Delta H^0 - \Delta G^0\right) / T\right) \quad \text{(S17)}$$

Here R is the universal gas constant with the value of 8.314 J mol^{-1} K^{-1} and T is the temperature in K[15]. The value of K_d can be determined from the slope of q_e versus C_e.[18,19] The plot of ln K_d versus $1/T$ was utilized to determine the value of ΔH^0 and ΔS^0.[20]

Table S12 Thermodynamic parameters for MG and Pb(II) adsorption on SiA-2 in single and binary component solution

Pollutant	K_d (L mol^{-1})			ΔG^0 (kJ mol^{-1})			ΔH^0 (kJ mol^{-1})	ΔS^0 (kJ mol^{-1})
	283 (K)	303 (K)	318 (K)	283 (K)	303 (K)	318 (K)		
MG in single component solution	1.02	1.92	6.89	-0.05	-1.64	-5.10	39.36	0.14
Pb(II) in single component solution	0.33	0.86	0.44	2.60	0.38	2.19	51.74	0.16
MG in binary solution	1.36	1.52	2.75	-0.73	-1.05	-2.67	14.11	0.05
Pb(II) in binary solution	1.12	1.31	1.40	-0.27	-0.69	-0.90	4.89	0.02

Regeneration

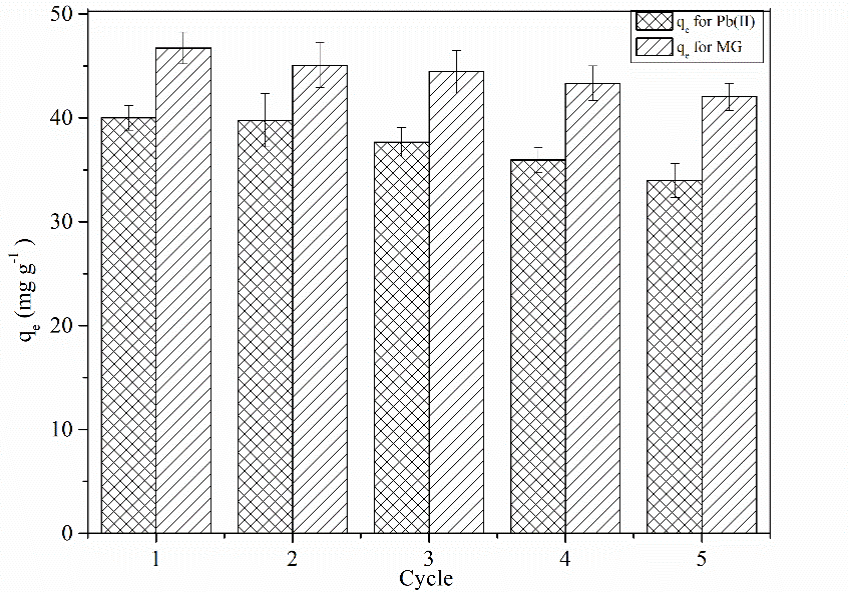

Fig. S11. Adsorption capacity of SiA-2 after reusing for different cycles for Pb(II) and MG (initial Pb(II) concentration: 40 mg L^{-1}; initial MG concentration: 50 mg L^{-1}; pH: 6; adsorbent dosage: 1 g L^{-1})

NOMENCLATURE

Symbols	Statement
%Adsorption	percent Pb(II) or MG removal
ΔG^0	Gibb's free energy change (kJ mol^{-1})
ΔH^0	enthalpy change (kJ mol^{-1})
ΔS^0	entropy change (kJ mol^{-1} K^{-1})
A	equilibrium of binding constant at the maximum binding energy (L g^{-1})
b	Langmuir adsorption constant
C	thickness of boundary layer in the equation of intra-particle diffusion model
C_0	initial Ni(II) concentration of the solution (mg L^{-1})
C_e	equilibrium Ni(II) concentration of the solution after adsorption (mg L^{-1})
k_1	rate constant for pseudo-first order adsorption (min^{-1})
k_2	rate constant for pseudo-second order adsorption (g mg^{-1} min^{-1})
K_c	equilibrium constant
K_f	Freundlich constants (related to adsorbent capacity)
k_{int}	rate constant of intra-particle diffusion model
m	mass of adsorbent per unit volume of solution (g)
n	Freundlich constants (adsorption intensity on the adsorbent)
q_e	amount of Pb(II) or MG uptake per unit amount of adsorbent (mg g^{-1})
q_m	maximum monolayer adsorption capacity (mg g^{-1})
q_t	mass of solute adsorbed on adsorbent (mg g^{-1}) at agitation time t
R	universal gas constant (J mol^{-1} K^{-1})
R_L	separation factor constant
RT/b_T	related to the heat of adsorption (J mol^{-1})
T	absolute temperature (K)
t	agitation time (min)
V	volume of solution (L)
α	initial adsorption rate (mg g^{-1} min^{-1})
β	desorption constant (mg g^{-1} min^{-1})

Reference

1 G. H. Bai, W. Teng, X. G. Wang, J. G. Qin, P. Xu and P. C. Li, *Trans. Nonferrous Met. Soc. China (English Ed).*, 2010, **20**, s169–s175.

2 B. Stuart, *Infrared Spectroscopy: Fundamentals and Applications*, John Wiely and sons, LTD, New Jersey, United States, 2004.

3 A. Asfaram, M. Ghaedi, S. Hajati, A. Goudarzi and A. A. Bazrafshan, *Spectrochim. Acta - Part A Mol. Biomol. Spectrosc.*, 2015, **145**, 203–212.

4 M. R. El-Naggar, A. M. El-Kamash, M. I. El-Dessouky and A. K. Ghonaim, *J. Hazard. Mater.*, 2008, **154**, 963–972.

5 Z. Sarbak, A. Stańczyk and M. Kramer-Wachowiak, *Powder Technol.*, 2004, **145**, 82–87.

6 K. Ojha, N. C. Pradhan and A. N. Samanta, *Bull. Mater. Sci.*, 2004, **27**, 555–564.

7 M. I. Khan, T. K. Min, K. Azizli, S. Su, H. Ullah, Z. Man, S. Sufian, H. Ullah and Z. Man, *RSC Adv.*, 2015, **5**, 61410–61420.

8 M. Rafatullah, O. Sulaiman, R. Hashim and A. Ahmad, *J. Hazard. Mater.*, 2009, **170**, 969–977.

9 S. Hajati, M. Ghaedi and S. Yaghoubi, *J. Ind. Eng. Chem.*, 2015, **21**, 760–767.

10 A. Chatterjee, J. K. Basu and A. K. Jana, *Powder Technol.*, 2019, **354**, 792–803.

11 L. Zhang, H. Zhang, W. Guo and Y. Tian, *Appl. Clay Sci.*, 2014, **93**–**94**, 85–93.

12 S. Ayhan, E. Bulut, M. Özacar and I. A. Şengil, *Microporous Mesoporous Mater.*, 2008, **115**, 234–246.

13 M. Ahmaruzzaman, *Adv. Colloid Interface Sci.*, 2011, **166**, 36–59.

14 S. Deng and Y. P. Ting, *Langmuir*, 2005, **21**, 5940–5948.

15 N. M. Mahmoodi, B. Hayati and M. Arami, *J. Chem. Eng. Data*, 2010, **55**, 4638–4649.

16 S. Wang and E. Ariyanto, *J. Colloid Interface Sci.*, 2007, **314**, 25–31.

17 H. Mazaheri, M. Ghaedi, A. Asfaram and S. Hajati, *J. Mol. Liq.*, 2016, **219**, 667–676.

18 M. F. Sawalha, J. R. Peralta-Videa, J. Romero-González and J. L. Gardea-Torresdey, *J. Colloid Interface Sci.*, 2006, **300**, 100–104.

19 Y. Liu, *J. Chem. Eng. Data*, 2009, **54**, 1981–1985.

20 Y. Liu, C. Yan, Z. Zhang, H. Wang, S. Zhou, W. Zhou, H. Wang, Y. Liu, W. Zhou, Z. Zhang, C. Yan, Z. Zhang, H. Wang, S. Zhou and W. Zhou, *Fuel*, 2016, **185**, 181–189.